Coupled As and Mn redox transformations in an Fe(0) electrocoagulation system: competition for reactive oxidants and sorption sites

Charlotte Catrouillet, Sachiko Hirosue, Nathalie Manetti, Victor Boureau, Jasquelin Peña

Environmental Science & Technology

pubs.acs.org/est

Article

Coupled As and Mn Redox Transformations in an Fe(0) Electrocoagulation System: Competition for Reactive Oxidants and Sorption Sites

Charlotte Catrouillet, Sachiko Hirosue, Nathalie Manetti, Victor Boureau, and Jasquelin Peña*

Cite This: *Environ. Sci. Technol.* 2020, 54, 7165−7174

Read Online

ACCESS | Metrics & More | Article Recommendations | Supporting Information

ABSTRACT: Iron electrocoagulation (EC) can be used for the decentralized treatment of arsenic(As)-contaminated groundwater. Iron EC involves the electrolytic dissolution of an Fe(0) electrode to Fe(II). This process produces reactive oxidants, which oxidize As(III) and Fe(II) to As(V) and a range of Fe(III) (oxyhydr)oxide phases. Here, we investigated the impact of manganese (Mn) on As removal, since the two often co-occur in groundwater. In the absence of Mn(II), we observed rapid As(III) oxidation and the formation of As(V)−Fe(III) polymers. Arsenic removal was achieved upon aggregation of the As(V)−Fe(III) polymers. In the presence of Mn, the mechanism of As removal varied with pH. At pH 4.5, As(III) was oxidized rapidly by $OH^{\bullet}$ and the aggregation of the resulting As(V)−Fe(III) polymers was enhanced by the presence of Mn. At pH 8.5, As(III) and Mn(II) competed for Fe(IV), which led As(III) to persist in solution. The As(V) that did form was incorporated into a mixture of As(V)−Fe(III) polymers and a ferrihydrite-like phase that incorporated 8% Mn(III); some As(III) was also sorbed by these phases. At intermediate pH values, As(III) and Mn(II) also competed for the oxidants, but Mn(III) behaved as a reactive intermediate that reacted with Fe(II) or As(III). This result can explain the presence of As(V) in the solid phase. This detailed understanding of the As removal mechanisms in the presence of Mn can be used to tune the operating conditions of Fe EC for As removal under typical groundwater conditions.

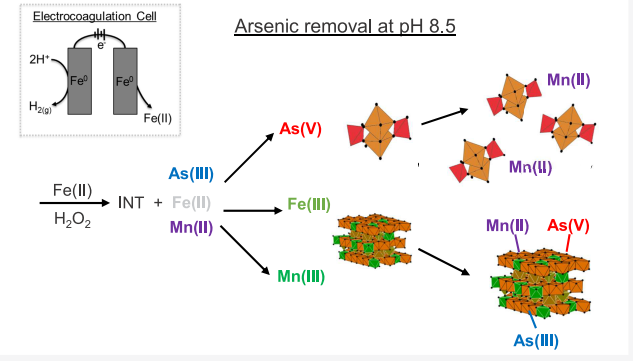

INTRODUCTION

Many low-resource regions have groundwater that is contaminated with arsenic (As), which must be effectively removed to provide safe drinking water. Among 14 different technologies that have been field-tested for removing As, iron electrocoagulation (EC) was rated as one of five technologies that meet international standards for As removal.[1] Overall, EC effectively removes As from groundwater to values below the recommendation from the World Health Organization (WHO) of 10 $\mu g\ L^{-1}$ (0.133 μM).[2−9] In particular, EC is attractive for use in decentralized communities because it has a short supply chain, low energy requirements, and is easy to operate.[10−14]

Arsenic removal in an EC system relies upon a number of redox reactions. First, electrical current is passed through an Fe(0) electrode to oxidize Fe(0) to Fe(II) at the anode. Subsequently, Fe(II) oxidation by O_2 and/or H_2O_2 generates reactive oxidant species, including hydroxyl radical ($OH^{\bullet}$), superoxide ($O_2^{\bullet-}$), and Fe(IV), which readily oxidize As(III) to As(V) and/or Fe(II) to Fe(III).[10,13−15] Iron(III) then polymerizes into Fe(III) (oxyhydr)oxides that adsorb As(III, V) in a pH-dependent manner. Both of these processes depend strongly on the chemical composition of the treatment water, especially the pH and concentration of co-occurring divalent cations and oxyanions. Both processes also produce a range of precipitates with varying affinities for As and ease of separation by filtration or settling.[4,5,10,16,17]

In many places, dissolved manganese (Mn) concentrations in groundwater range from 0.27 to 103 μM and can be 5500-fold greater than As concentrations (0.01−60 μM As, Figure S1).[18−28] In EC experiments conducted in the absence of As, van Genuchten and Peña[29] showed that Mn(II) was oxidized to Mn(III) and incorporated into the resulting Fe(III) (oxyhydr)oxides. The extent of Mn removal during EC varied with the solution pH and initial oxidant (O_2 vs H_2O_2). While the mechanisms of As and Mn removal by EC have been studied separately, no published work has investigated the redox and sorption reactions that underpin EC performance in waters where As and Mn co-occur and where EC precipitates

Received: November 22, 2019
Revised: April 28, 2020
Accepted: May 4, 2020
Published: May 4, 2020

are generated in situ in the presence of both As and Mn. We expect that Mn can influence As removal by EC by three mechanisms. First, because Mn(II) can be oxidized by superoxide ($O_2^{\bullet-}$),[30−34] hydroxyl radical ($OH^{\bullet}$),[29] oxygen (O_2),[34] and Fe(IV)[29,35] (Figure S2), it may scavenge the reactive oxidant species generated from Fe(II) oxidation and limit the oxidation of As(III) to As(V). Second, the incorporation of Mn into Fe oxides can modify the ability of the EC precipitates to adsorb As(III, IV).[29,36−38] Third, Mn(III) produced by EC may oxidize As(III) to As(V).[39−41]

In the current study, we investigated the extent and mechanism of As removal by EC in the presence of Mn(II). Since available field measurements show that Mn concentrations commonly exceed As concentrations in groundwater (Figure S1), we conducted our experiments at Mn:As concentration ratios of 10:1 and 1:1 and at total Mn and As concentrations where analytical and spectroscopic analyses could be readily performed. Kinetic experiments at pH 4.5−8.5 were conducted under four initial conditions: 10 μM of As(III) and 0 μM of Mn(II) [10As0Mn], 10 μM of As(III) and 100 μM of Mn(II) [10As100Mn], 100 μM of As(III) and 0 μM of Mn(II) [100As0Mn], and 100 μM of As(III) and 100 μM of Mn(II) [100As100Mn]. Additionally, 250 μM of H_2O_2 was added to the experiments because (i) it favors the Fenton reactions that generate $OH^{\bullet}$ and Fe(IV) instead of $O_2^{\bullet-}$, which does not oxidize As(III) at appreciable rates relative to $OH^{\bullet}$ and Fe(IV),[15] and (ii) it precipitates disordered or nanoscale Fe(III) oxides with a high capacity to sorb As.[42] In the dissolved phase, the concentrations of As(III) and As(V) in solution were determined by combining hydride generation inductively coupled plasma optical emission spectrometry (HG-ICP-OES) and ICP-OES. Dissolved Fe and Mn concentrations were also determined by ICP-OES. In the solid phase, the redox speciation of As, Mn, and Fe was determined using X-ray Absorption Near-Edge Structure (XANES) spectroscopy at the As, Mn, and Fe K-edges. Finally, Extended X-ray Absorption Fine Structure (EXAFS) spectroscopy was used to determine the structure of the precipitates formed; this included the potential incorporation of Mn(III) as well as the As oxidation state and binding mode in the solid phase. This work shows how coupled As, Mn, and Fe redox transformations impact As oxidation and sorption by Fe(III) phases generated by EC, which is critical for treating groundwater with co-occurring As and Mn.

MATERIALS AND METHODS

All solutions were prepared using 18.2 MΩ cm deionized water and ACS-grade reagents.

Kinetics of As(III) and Mn(II) Removal. A description of the Fe(0) EC cell[16] used for kinetic experiments is provided in the Supporting Information (SI). Briefly, experiments were initiated by applying galvanostatic currents of 6 mA to the electrodes (Table S1) in 2 mM NaCl and 2 mM $NaHCO_3$. According to Faraday's law, Fe = $(I \times t_e)/(n \times F)$, where Fe (mol) is the amount of Fe generated during EC, I (C s^{-1}) is the current, t_e is the electrolysis time (s), n is the number of transferred electrons, and F is Faraday's constant (96 485 C mol^{-1}). With a volume of 250 mL, Fe(II) was produced at a rate of about 7 μM min^{-1}. This Fe production rate was chosen (i) to minimize Fe(II) accumulation and thus maximize the consumption of reactive oxidant species by Mn(II) and As(III), and (ii) to compare with previous data from our group.[10,29] Current was applied for 32 min, and samples were collected at 0, 6, 13, 23, and 32 min.

Triplicate experiments were conducted at pH 4.5, 6.5, and 8.5 using initial concentrations of 250 μM of H_2O_2, 10 or 100 μM of As(III) ($NaAsO_2$; Fisher Chemical), and 0 or 100 μM of Mn(II) ($MnCl_2{\cdot}4H_2O$; Sigma-Aldrich). Hereafter, experiments are identified by the initial As and Mn concentrations. Data for experiments conducted in the absence of As (i.e., 0As100Mn) were obtained previously using the same setup and similar experimental conditions.[29] Samples were collected to analyze the total and dissolved concentrations of As, Mn, and Fe. For total concentrations, 2 mL was sampled. For dissolved phase concentrations, 4−5 mL were sampled, and the first mL of the filtrate was discarded. Filtration was performed using 0.22 μm of PES BGB or 0.02 μm of Whatman Anotop syringe filters in a small subset of experiments. Samples were also collected by filtration for X-ray absorption spectroscopy (XAS).

Chemical Analysis. Arsenic, Mn, and Fe concentrations were determined using a PerkinElmer Optima 8300 ICP-OES as summarized in Table S2. Total As concentrations below 3 μM and As(III) concentrations in the dissolved phase were determined using HG-ICP-OES (see the SI).[43] Aqueous As(V) concentrations were determined from the difference between total As and As(III) concentrations. Aqueous Mn in our experiments can only be present as Mn(II) because $Mn(III)_{(aq)}$ must be stabilized by high-affinity ligands, which are not present in our experiments. While aqueous Fe can be present as Fe(II) or Fe(III), Fe(II) is a minor component in our system, as indicated from experiments using 0.02 mm filters (see Results) and calculations based on our experimental conditions and published rate constants for Fe(II) oxidation to Fe(III) by H_2O_2 (up to 80 M^{-1} s^{-1} at all pH values)[44−47] and by O_2 (0.19 and 548 M^{-1} s^{-1} at pH 6.5 and 8.5, respectively, as calculated from data in Millero et al.).[44] These calculations are described in the SI and Table S3. Throughout the text, As removal refers to the removal of As from the dissolved phase to the solid phase, where As can be sorbed to the Fe(III) (oxyhydr)oxides as As(III) [As(III) sorbed] and/or As(V) [As(V) sorbed]. Manganese removal is defined similarly, although Mn can be sorbed as Mn(II) or Mn(III) or incorporated into the precipitates as Mn(III) or Mn(IV).

X-ray Absorption Spectroscopy. Samples for XAS analysis were collected by filtration onto 0.45 μm filter membranes (25 mm diameter, nitrocellulose filter; Millipore Sigma Aldrich). The membranes were then coated with a drop of glycerol (50%) to prevent As(III) oxidation, cut into 4−5 rectangular sections, arranged in a stack, and then sealed with Kapton tape. The sealed sample was attached to an aluminum sample holder and immediately frozen to prevent As(III) oxidation. Samples were stored at −20 °C until analysis.

Iron, As, and Mn K-edge X-ray absorption (XA) spectra were collected at 77 K (LN_2 cryostat) at the Stanford Synchrotron Radiation Laboratory (BL 4-1) using a Si(220) ϕ = 90 monochromator crystal. The incident beam (1 mm in the vertical dimension) was detuned by 35, 50, and 50% for As, Mn, and Fe, respectively. Monochromator energies were calibrated using metal foils: 7112 eV (Fe), 11,919 eV (Au), and 6,539 eV (Mn). Iron K-edge XA spectra were collected in transmission mode using ion chambers for measuring I_0 and I_t. Arsenic K-edge XA spectra were collected in transmission or fluorescence mode, whereas Mn K-edge XA spectra were collected in fluorescence mode. Fluorescence yield spectra

https://dx.doi.org/10.1021/acs.est.9b07099
Environ. Sci. Technol. 2020, 54, 7165−7174

were measured using a solid-state passivated implanted planar silicon (PIPS) detector, a Lytle detector equipped with Soller slits, or a Ge detector equipped with Z-1 filters (i.e., Ge for As and Cr for Mn).

The data reduction followed standard procedures.[13,29] Replicate scans (2−6) were averaged to improve the signal-to-noise ratio, and the dead-time was corrected when acquired using the Ge detector. No X-ray-induced changes were observed between replicate scans. X-ray absorption spectra were averaged, background-subtracted (E_0 values of 6550, 11 875, and 7127 eV for Mn, As, and Fe, respectively), and normalized to 1 absorption unit. The extracted EXAFS spectra were weighted by k^3 and Fourier-transformed (FT) using a Kaiser−Bessel window with a dk value of 3 Å^{-1}. Both XANES and EXAFS spectra were compared to reference spectra acquired from samples with Fe, As, and Mn in known oxidation states (Table S4). Arsenic and Mn K-edge XANES and Fe K-edge EXAFS spectra were subsequently analyzed by linear combination fitting (LCF) in SixPack as described in detail in the SI and in Tables S5−S7.[48]

RESULTS

Arsenic(III) Removal by EC in the Absence of Mn(II). The kinetics and extent of As removal in a NaCl/$NaHCO_3$ electrolyte solution are shown in Figure 1A (A-1 to A-3) and Figure 1B (B-1 to B-3). In the 10As0Mn experiments at pH 4.5 and 6.5, the dissolved As concentration was below the 10 μg L^{-1} or 0.133 μM WHO recommendation after 32 min of EC (Figure 1A (A-1 and A-2)). In the pH 8.5 10As0Mn experiment, however, 0.2 μM of As remained in solution, which exceeds the WHO recommendation (Figure 1A (A-3)). In the 100As0Mn experiments, the WHO recommendation was reached only at pH 4.5. At pH 8.5 and 6.5, dissolved As concentrations largely exceeded the WHO recommendation, with 23.2 and 80.7 μM of As remaining in solution (Figure 1B (B-1 to B-3)).

In general, As removal from the dissolved phase was enhanced by decreasing the pH and increasing the amount of Fe in the solid phase (Figure 1A (A-1 to A-3) and Figure 1B (B-1 to B-3) and Figure 2A (A-1 to A-3) and Figure 2B (B-1 to 2B-3); Table S8). While As removal started immediately at pH 4.5, the onset of As removal was progressively delayed with increasing pH and increasing initial As concentration. For instance, in the 10As0Mn experiments, As removal was not observed or was minimal until 6 and 13 min at pH 6.5 and 8.5, respectively (<20% As removed, Figure 1A (A-2 and A-3)). In the 100As0Mn experiments, removal was observed starting at 13 and 23 min at pH 6.5 and 8.5, respectively (<10% As removed, Figure 1B (B-2 and B-3)). The poorer removal of As at higher pH values and/or higher As concentrations cannot be explained by the limited oxidation of Fe(II) to Fe(III) or As(III) to As(V). Excess H_2O_2 was available in these experiments, and As(III) and Fe(II) are readily oxidized in the presence of H_2O_2 at pH 4.5−8.5.[15] Additionally, As(V) was the dominant or exclusive form of As in all samples at $t > 6$ min (Figure 1A (A-1 to A-3) and Figure 1B (B-1 to B-3)), and our calculations predict small to negligible Fe(II) (Table S3). The apparent contradiction in the data regarding Fe(III) formation and As(V) removal can be explained by a shift in the mechanism of Fe(III) polymerization, which prevents the formation of As(V)−Fe(III) precipitates[49] that can be removed by filtration (0.22 μm).

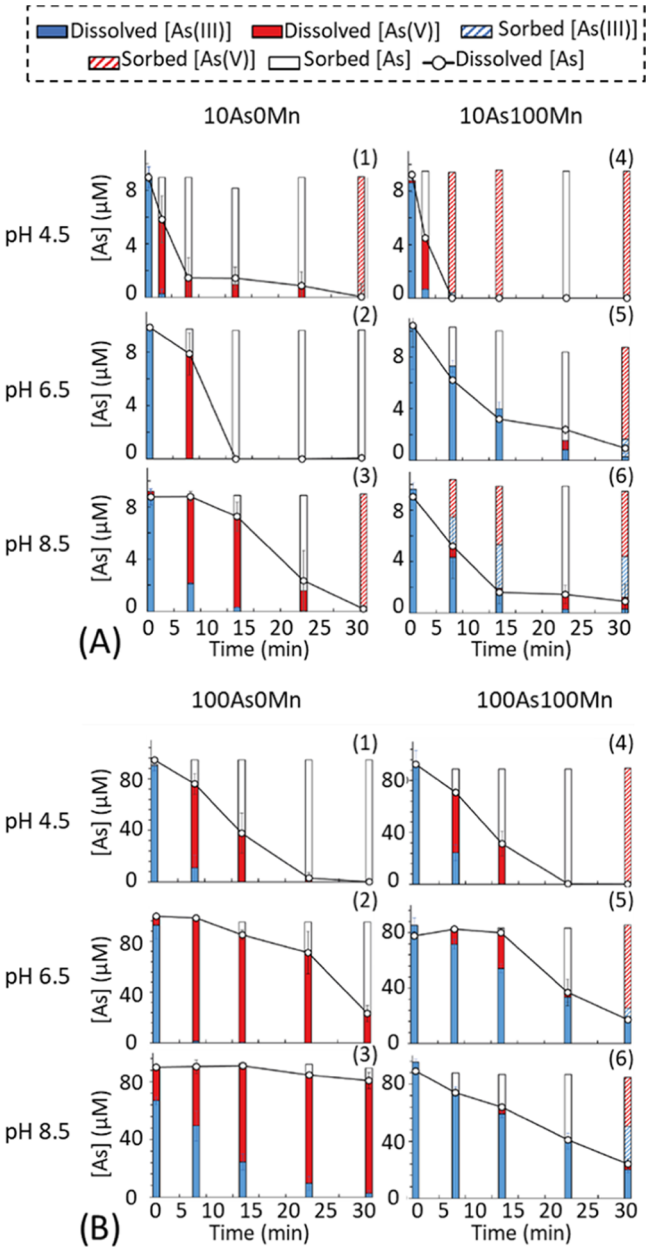

Figure 1. Arsenic (As) removal from solution in the presence of Manganese (Mn) plotted as a function of time and pH for experiments with (A) 10 μM of As(III) and 0 or 100 μM of Mn(II) (i.e., 10As0Mn and 10As100Mn, respectively) and (B) 100 μM of As(III) and 0 or 100 μM of Mn(II) (i.e., 100As0Mn and 100As100Mn, respectively). Bars show the concentrations of As(III) (blue) and As(V) (red) in the dissolved phase (solid bars) and solid phase (shaded bars).

At pH 6.5 and 8.5, the large fraction of dissolved As(V) (Table S8) coincided with the large fraction of dissolved Fe (Table S8). For example, at pH 8.5 in the 10As0Mn experiments, 73% of the As and 70% of the Fe were in the dissolved phase at 13 min. Additionally, the higher percentages of dissolved As(V) and dissolved Fe in the 100As0Mn experiments at later time points (e.g., 76% As(V) and 78% Fe at 23 min) relative to the 10As0Mn experiments (e.g., 17% As(V) and 17% Fe at 23 min) indicate that high As/Fe ratios favor the accumulation of Fe in the dissolved phase, as similarly observed by Shi et al.[50] Complementary experiments using

https://dx.doi.org/10.1021/acs.est.9b07099
Environ. Sci. Technol. 2020, 54, 7165−7174

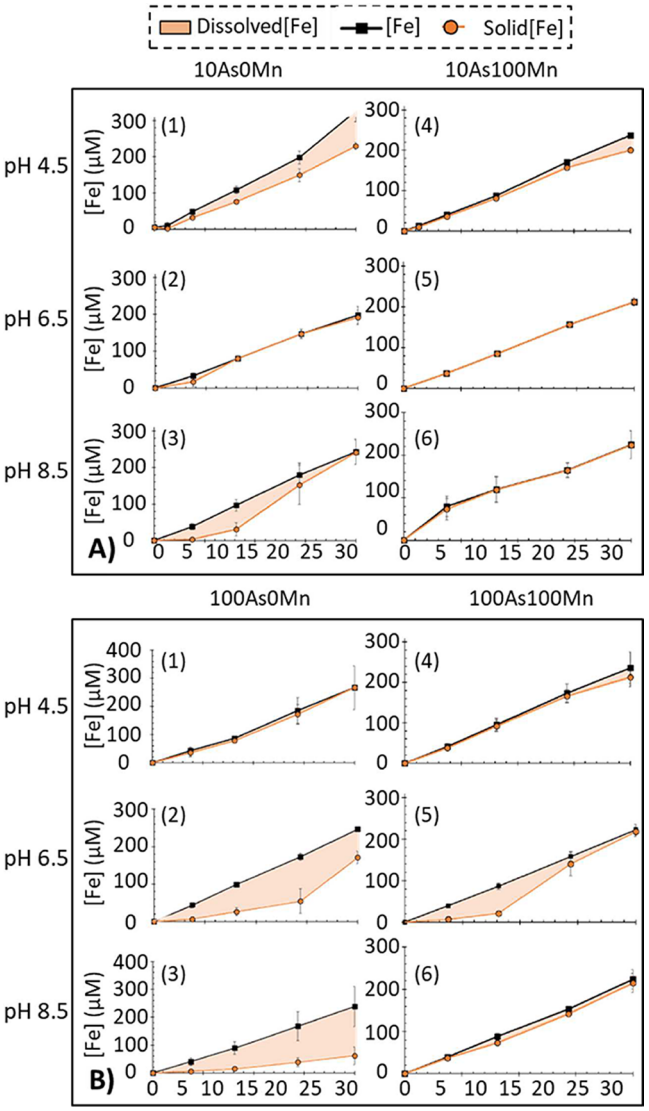

Figure 2. Concentration of total iron (Fe) added into the reactors as Fe(II) (black markers) and in the solid phase as Fe(III) (orange markers) plotted as a function of time and pH for experiments with (A) 10 μM of As(III) and 0 or 100 μM of Mn(II) (i.e., 10As0Mn and 10As100Mn, respectively) and (B) 100 μM of As(III) and 0 or 100 μM of Mn(II) (i.e., 100As0Mn and 100As100Mn, respectively). The shaded areas show the difference between the total Fe in the reactors and in the solid phase (orange markers). Iron concentrations were determined by ICP-OES.

0.02 μm and 0.2 μm filters showed that most of the dissolved Fe and a large fraction of the dissolved As(V) were contained in the 0.02−0.20 μm size fraction. For example, 100 and 92% of the Fe and 86 and 37% of the As were present in the 0.2−0.02 μm size fraction in samples collected at 6 min from the 10As0Mn experiments at pH 6.5 and 8.5, respectively (Figure S3). Experimental results are thus consistent with the formation of As(V)−Fe(III) polymers, especially at short reaction times when the As(V):Fe(III) ratio is high (e.g., As[V]:Fe[III] ratios of 2.62 at pH 6.5 and 1.2 at pH 8.5 in the 100As100Mn experiments at 6 min). The formation of As(V)−Fe(III) polymers is also more favorable at higher pH values since the kinetics of Fe(II) oxidation by Fe(IV) are fast[51] and Fe(IV) is the dominant oxidant (Figure S4).

Furthermore, as the pH increased from 6.5 to 8.5, the As/Fe ratio in the 0.2−0.02 μm fraction decreased from 0.3 to 0.1 in samples taken after 6 min in the 10As0Mn experiments (Figure S3). Thus, the sorption capacity of the Fe(III) polymers decreased with increasing pH, as is typically observed for Fe(III) oxides. However, we cannot exclude the presence of aqueous As species, especially at pH 8.5, where 24% of the As was present as As(III) at 6 min.

Oxyanion−Fe(III) polymers containing oxyanion:Fe(III) ratios of 0.5 and 0.7 mol mol^{-1} have been described[16,52] for arsenate and phosphate, respectively. In the 10As0Mn experiments, all samples had As:Fe ratios below 0.7 in the dissolved phase, which indicates that the pool of dissolved Fe(III) was sufficient to trap all of the dissolved As (Table S8). For the 100As0Mn samples, instead, the As(V) concentrations exceeded the dissolved Fe concentrations in samples collected at t < 13 min (Table S8). Thus, in these experiments, dissolved As likely occurs both as free As and Fe(III)-bound As.

At pH 4.5, the nearly complete oxidation of As(III) to As(V) observed in the first minutes of the experiments should favor the formation of As(V)−Fe(III) polymers, especially in 100As0Mn experiments where the As(V)/Fe(III) ratios are initially high. However, dissolved Fe concentrations decreased as the initial As concentrations increased from 10 to 100 μM (Figure 2A (A-1) and Figure 2B (B-1); Table S8). The wet chemical data, therefore, provide no evidence for the presence of As(V)−Fe(III) polymers in solution at low pH values. However, Fe K-edge EXAFS spectra measured from the solid phase and transmission electron micrographs (Figure S12) suggest that the polymers formed and were rapidly removed from solution upon aggregation, as described below.

Influence of Mn on As(III) Removal by EC. The kinetics of As removal by EC in the presence of 100 μM of Mn(II) and low (10As100Mn) or high (100As100Mn) initial As(III) concentrations are shown in Figure 1A (A-4 to A-6) and Figure 1B (B-4 to B-6). After 32 min, dissolved As concentrations were below the 10 μg L^{-1} or 0.133 μM WHO recommendation only in the pH 4.5 experiments (Figure 1A (A-4) and Figure 1B (B-4)). Instead, the dissolved phase contained 0.9, 17.3, and 24.2 μM of As, respectively, after 32 min for the pH 6.5 10As100Mn, 6.5 100As100Mn, and 8.5 100As100Mn conditions (Figure 1A (A-5) and Figure 1B (B-5 and B-6)). In the pH 8.5 10As100Mn experiment, while 82% of the total added As was removed after 13 min, the dissolved As concentrations remained relatively constant and above the WHO recommendation at about 1.30 μM between 13 and 32 min (Figure 1A (A-6)).

Similar to experiments conducted in the absence of Mn, As(III) oxidation and removal were most efficient at pH 4.5, with more than 65% (2 min) and 85% (6 min) of the As in solution present as As(V) in the 10As100Mn and 100As100Mn experiments, respectively (Figure 1A (A-4) and Figure 1B (B-4)). In these experiments, the oxidation of As(III) to As(V) by OH$^{\bullet}$,[15] which represents 81% of the oxidant species (Figure S4), was favorable despite the presence of 100 μM of Mn(II) in solution. Arsenic(III) oxidation could also have been mediated by Mn(III, IV)[53] if Mn(II) oxidation by OH$^{\bullet}$[54,55] were faster than As(III) oxidation. Additionally, faster As removal from the dissolved phase occurred in the presence of Mn (10As100Mn; Figure 1A (A-4)) than in its absence (10As0Mn, Figure 1(A-1)). As discussed below, Mn and Fe K-edge XANES and EXAFS spectra from the solid phase suggest that Mn enhanced As removal by screening the

https://dx.doi.org/10.1021/acs.est.9b07099
Environ. Sci. Technol. 2020, 54, 7165−7174

negative charge of As(V) sorption complexes on the Fe(III) oxyhydroxides and enhancing aggregation.[16,17,52]

At pH 6.5 and 8.5, dissolved As remained dominantly as As(III), which is in sharp contrast to the experiments conducted in the absence of Mn (Figure 1A (A-2 and A-3; A-5 and A-6) and Figure 1B (B-2 and B-3; B-5 and B-6)). For example, at pH 6.5, 100% As(V) and 100% As(III) were measured in the filtrates of samples collected at 6 min in the 10As0Mn and 10As100Mn experiments, respectively (Figure 1A (A-2 and A-5)). Similar trends were observed at pH 8.5 after 6 min, where 76% As(V) and 84% As(III) were measured in the dissolved phase for 10As0Mn and 10As100Mn experiments, respectively (Figure 1A (A-3 and A-6)).

The stabilization of As(III) in As(III)−$Mn(II)_{(aq)}$ complexes cannot explain its limited oxidation since As(III)−$Mn(II)_{(aq)}$ species are not thermodynamically favorable (Figure S5). Instead, we inferred that Mn(II) outcompetes As(III) for Fe(IV), which is the dominant oxidant at pH > 5.5. Consistent with this hypothesis, significant Mn removal from the dissolved phase occurred at pH 8.5 (58.14 and 53.52 μM in the 10As100Mn and 100As100Mn experiments, respectively; Table S8). At pH 6.5, however, if Mn(II) was oxidized to Mn(III), Mn(III) must be a short-lived intermediate because little Mn was sorbed to the solid phase after 32 min (3.99 and 2.31 μM in 10As100Mn and 100As100Mn, respectively; Table S9). Notwithstanding the predominance of dissolved As(III), both As and Fe were steadily removed from the solution, with the exception of the pH 6.5 100As100Mn experiment.

In the pH 6.5 100As100Mn experiment, the onset of As removal was delayed and occurred at $t \geq 13$ min (Figure 1B (B-5)). This delay coincided with high dissolved Fe and As(V) concentrations at $t \leq 13$ min and As/Fe ratios ranging from 1.2 to 3.9 (Figure 1B (B-5) and Figure 2B (B-5); Table S8). Additionally, no Mn was removed from the solution at $t \leq 13$ min. The presence of both As and Fe in solution is consistent with the formation of As(V)−Fe(III) polymers, which we also identified at pH 6.5 in the absence of Mn.

Structure of Fe(III) Precipitates Formed by EC. The Fe K-edge EXAFS spectra and corresponding FT of all samples and reference spectra are plotted in Figure S6, with experimental samples grouped according to solution pH. Qualitative comparison of the Fe K-edge EXAFS spectra and FT from the samples and references shows that the generated EC precipitates have a significantly less ordered structure than that of goethite or lepidocrocite. Additionally, principal component analysis (PCA) and target transform analysis[56] using three components (cumulative variance of 0.87) returned good spoil values for Fh (2.2) and HFO-Si[17] (2.9). An excellent spoil value was also returned for the 32 min sample from the pH 4.5 100As100Mn experiment (1.1), which was excluded from the PCA run. This sample showed very weak Fe−Fe scattering in the FT, indicating that it is in a highly disordered phase (Figure S6). Based on the high As/Fe ratios and low pH, which are favorable for As(V) sorption to Fe(III)[42] but unfavorable for the growth of ordered precipitates,[57] we assume that this sample consists largely of the oxyanion−Fe(III) polymers described in the literature.[16,52] This sample contains an As(V)/Fe(III) ratio of 0.42, which is close to the 0.5 ratio reported for polymers formed in the presence of phosphate and lower than the 0.7 ratio for As(V) in the presence of Ca. Hereafter, this sample is interpreted as an As(V)−Fe(III) polymer phase and its EXAFS spectrum is used as a reference sample in LCF.

For the Fe K-edge EXAFS spectra shown in Figure S6, the best LCF results were obtained using Fh and the As(V)−Fe(III) polymer phase as references, as determined from the high sum of components (94−101%) and low *R*-factors (<0.02) (Table S6). The polymer fraction represented at least 36% of the solid phase across all samples, although the percentages varied with the reaction time and pH (Figures 3d−f and S7). For instance, the 32 min samples from the

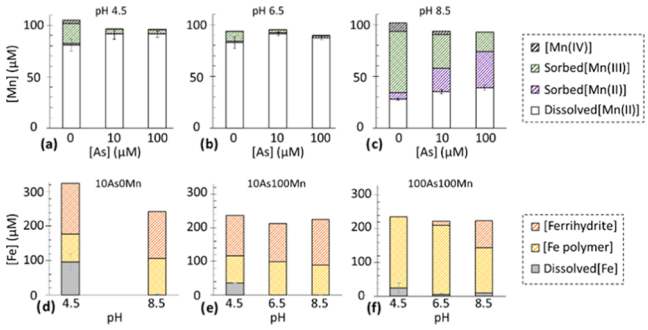

Figure 3. Concentrations and speciation of (a−c) Mn and (d−f) Fe after 32 min in the dissolved phase (solid bars) and solid phase (shaded bars). For Mn, data are presented as a function of the initial As concentrations for experiments conducted at (a) pH 4.5, (b) 6.5, and (c) 8.5. For Fe, data are presented as a function of pH for experiments conducted with (d) 10As0Mn, (e) 10As100Mn, and (f) 100As100Mn.

10As0Mn and 10As100Mn experiments had 50 to 60% Fh and 36 to 44% As(V)−Fe(III) polymers, respectively. As expected, the 100As100Mn samples (32 min), which had higher initial As concentrations and thus larger As/Fe ratios, showed a 100 to 61% contribution of the polymer phase (Table S6). Larger proportions of the polymer phase were also observed at short reaction times, which had the highest As(V)/Fe(III) ratios. For example, the polymer phase accounted for 79% at 6 min and 39% at 32 min in the pH 4.5 10As100Mn experiment. Finally, in the 100As100Mn experiments, the contribution of the polymer phase decreased from 100 to 61% as pH increased from 4.5 to 8.5 (32 min), which is correlated with an increase in the polymer fraction in the dissolved phase (Table S8).

Overall, the fraction of the polymer phase in the precipitates correlated positively with the fraction of As(V) in the solid phase and inversely with the occurrence of As(V)−Fe(III) polymers in the dissolved phase. However, we note that the fitted polymer fraction, which we assumed to have an average As(V)/Fe(III) ratio of about 0.42, overestimates the true contribution of the polymer fraction in the pH 4.5, 6.5, and 8.5 10As100Mn, and pH 6.5 100As100Mn samples. For example, if all of the As in the 10As100Mn precipitates was contained in the polymer phase, the fitted fraction should be about 10% instead of 30%. Thus, highly disordered Fe(III) phases may also form due to the fast oxidation of Fe(II) in the presence of H_2O_2 as corroborated by experiments using H_2O_2 and O_2 as the primary oxidants. These experiments led to the formation of ferrihydrite- and lepidocrocite-like phases, respectively.[29]

Arsenic Speciation in the Absence and Presence of Mn(II). The oxidation state of As in the solid phase was determined by LCF analysis of As K-edge XANES and EXAFS spectra, wherein the values generally fell within 10% of each other (Figure S8 and Table S5). To represent the data, the As(V) and As(III) fractions were scaled to the amount of As in the solid phase, and are depicted by the hatched symbols in

https://dx.doi.org/10.1021/acs.est.9b07099
Environ. Sci. Technol. 2020, 54, 7165−7174

Figure 1. Samples from the 10As0Mn experiments at pH 4.5 and 8.5 contained As(V) in both the solid and dissolved phases, indicating quasi-complete oxidation of As in the absence of Mn (Figure 1A (A-1 and A-3)). In the presence of Mn at pH 4.5, As occurred as As(V) in the precipitates (Figure 1A (A-4) and Figure 1B (B-4)). In the presence of Mn at pH 6.5 and 8.5, however, about 16% (32 min) and 40% (6, 13, and 32 min), respectively, of the As in the solid phase were present as As(III) (Figure 1A (A-5 and A-6) and Figure 1B (B-5 and B-6)).

Manganese Uptake and Redox Speciation Determined by Mn K-edge XANES and EXAFS Spectroscopy. The Mn K-edge XANES spectra of the precipitates collected at 32 min were compared to a suite of Mn(II), Mn(III), and Mn(IV) reference compounds. Linear combination fits reproduced the experimental samples well (R-factor < 6×10^{-4} and component sum of 93−102%) and showed that Mn was present as Mn(III) and/or Mn(II). These fits also indicated that the contribution of each Mn species varied with the initial As(III) concentration and pH (Figures 3a−c and S9; Table S7). The amount of Mn(III) in the precipitates decreased as the initial As(III) concentration increased. Additionally, the amount of Mn(III) in the precipitates was greater at pH 4.5 than those at pH 6.5 and pH 8.5 than that at pH 6.5. The amount of Mn(III) in the precipitates decreased from 19.26 (no As(III)) to 3.66 (100 μM of As(III)) at pH 4.5 and from 59.07 (no As(III)) to 18.46 μM of Mn(III) (100 μM of As(III)) at pH 8.5. These trends are consistent with the competition between Mn(II) and As(III) for reactive oxidants and indicate different reactive oxidants at acidic and alkaline pH values.[29] Instead, the amount of Mn(II) in the solid phase generally increased with the initial As(III) concentration and the pH. This trend was most notable at pH 8.5, in which the precipitates showed 6.03 in the absence of As(III) and up to 35.06 μM of Mn(II) in the presence of 100 μM of As(III). Across all samples, Mn(IV) was a minor component (≤11%, up to 3.06 μM) and is, therefore, not discussed further.

The Mn K-edge EXAFS spectra and corresponding FT for the precipitates are shown in Figures S6, S10, S11. Similar peak positions and amplitudes in the EXAFS spectra and FT from precipitates that contained predominantly Mn(III) (i.e., pH 4.5 samples) match the EXAFS spectra from the 0As100Mn samples, where Mn was incorporated into the Fe(III) oxyhydroxides (Figure S6).[29] Conversely, for precipitates containing predominantly Mn(II) (i.e., pH 8.5 samples), the EXAFS spectra and FT are dominated by a single oscillation and show no evidence for a Mn−Mn/Fe second shell in the FT (Figure S10), suggesting that Mn(II) adsorbs primarily via nonspecific interactions (e.g., outer-sphere complexes).[34]

DISCUSSION

Oxidation of As(III) to As(V) in the Absence and Presence of Mn. *Arsenic(III) Oxidation by $OH^{\bullet}$ and Possibly Mn(III, IV) at pH 4.5.* At pH 4.5, where $OH^{\bullet}$ is the dominant oxidant (Figure S4), we observed fast and complete oxidation of As(III) to As(V) in the absence and presence of 100 μM of Mn. Additionally, the amount of Mn(III) associated with the solid phase decreased from 19.3 to 4.2 to 3.7 μM as the initial As(III)/Mn(II) molar ratio increased from 0 to 0.1 to 1.0. In the 10As100Mn experiments, where the initial Mn(II):As(III) ratio was 10, As(V) concentrations were around twice as high as the Mn(III) concentrations after 32 min of EC. These results are consistent with the rate constant for As(III) oxidation by $OH^{\bullet}$ (eqs 1 and 2), which is more than an order of magnitude higher than the rate constants for Fe^{2+} (eq 3) and Mn^{2+} (eq 4). These results also suggest that the rate constant for Mn(II) oxidation by $OH^{\bullet}$ is at least an order of magnitude lower than 8×10^9

$$\mathrm{As(III)} + \mathrm{OH}^{\bullet} \rightarrow \mathrm{As(IV)}, \quad k = 8 \times 10^9\ \mathrm{M^{-1}\,s^{-1}} \tag{1}$$

$$\mathrm{As(IV)} + \mathrm{O_2} \rightarrow \mathrm{As(V)} + \mathrm{O_2}^{\bullet -}, \quad k = 1.1 \times 10^9\ \mathrm{M^{-1}\,s^{-1}} \tag{2}$$

$$\mathrm{Fe^{2+}} + \mathrm{OH}^{\bullet} \rightarrow \mathrm{Fe^{3+}} + \mathrm{OH^-}, \quad k = 3.2 \times 10^8\ \mathrm{M^{-1}\,s^{-1}} \tag{3}$$

$$\mathrm{Mn^{2+}} + \mathrm{OH}^{\bullet} \rightarrow \mathrm{Mn^{3+}} + \mathrm{OH^-}, \quad k \geq 1.4 \times 10^8\ \mathrm{M^{-1}\,s^{-1}} \tag{4}$$

$$\mathrm{Mn(II)} + \mathrm{O_2}^{\bullet -} + 2\mathrm{H^+} \rightarrow \mathrm{Mn(III)} + \mathrm{H_2O_2}, \quad k = 4.2 \times 10^6 \times [\mathrm{H^+}]^2\ \mathrm{M\,s^{-1}} \tag{5}$$

Note: eqs 1−5 are from refs 15, 56, 32, respectively.

Any Mn(III, IV) formed transiently in solution and/or incorporated into the Fe oxides upon the reaction of Mn^{2+} with $OH^{\bullet}$ or $O_2^{\bullet -}$ should also oxidize As(III),[36] but this mechanism cannot be ascertained from the experimental data.

Arsenic(III) Oxidation by Fe(IV) at pH 6.5 and 8.5. The speciation of dissolved As showed a marked shift from As(V) at pH 4.5 to As(III) at pH 6.5 and 8.5 in the presence of Mn. At pH > 5.5, Fe(IV) is the dominant oxidant in the EC system (Figure S4), although if Mn(III, IV) formed, it would oxidize Fe(II) and As(III) to Fe(III) and As(V), respectively, with a concomitant reduction of Mn(III, IV) to Mn(II).[58] As shown by Hug and Leupin,[15] the kinetics of As(III) oxidation in the presence of Fe(II) depend strongly on the Fe(II) speciation, given the difference of 5 orders of magnitude in the rate constants for Fe^{2+} versus $FeOH^+$ oxidation by Fe(IV)

$$\mathrm{As(III)} + \mathrm{Fe(IV)} \rightarrow \mathrm{As(IV)} + \mathrm{Fe^{3+}}, \quad k = 4.2 \times 10^5\ \mathrm{M^{-1}s^{-1}} \tag{6}$$

$$\mathrm{Fe^{2+}} + \mathrm{Fe(IV)} \rightarrow 2\mathrm{Fe^{3+}}, \quad k = 1.9 \times 10^3\ \mathrm{M^{-1}s^{-1}} \tag{7}$$

$$\mathrm{FeOH^+} + \mathrm{Fe(IV)} \rightarrow 2\mathrm{Fe^{3+}}, \quad k = 1.4 \times 10^8\ \mathrm{M^{-1}s^{-1}} \tag{8}$$

Note: eqs 6−8 are from ref 15.

At pH 6.5 and in the absence of Mn, the rapid oxidation of As(III) to As(V) is consistent with these rate constants. In the presence of Mn, however, dissolved As remained largely as As(III), and little Mn(III) was detected in the solid phase (Figure 3b and Table S9). The persistence of As(III) and absence of Mn(III) at pH 6.5 suggest both that the rate constant for Mn^{2+} or $MnOH^+$ oxidation by Fe(IV) is larger than the rate constant for As(III) (eq 6) and that the Mn(III) generated upon the reaction with Fe(IV) is consumed rapidly by the reaction with Fe(II) to form Fe(III). This mechanism implies faster oxidation of Fe^{2+} by Mn(III, IV) than that of As(III) oxidation by Fe(IV) (eq 6). In other words, small amounts of oxidized Mn can enhance Fe oxidation at the expense of As oxidation. Nonetheless, 84−88% of the solid-phase As was present as As(V) after 32 min, which indicates that As(III) oxidized by Fe(IV) and/or Mn(III) in solution is

https://dx.doi.org/10.1021/acs.est.9b07099
Environ. Sci. Technol. 2020, 54, 7165−7174

sorbed immediately and/or that As(III) undergoes surface-catalyzed oxidation.

At pH 8.5, the competition between As(III) and Mn(II) for Fe(IV) was more evident than that at pH 6.5 due to the increase in Mn(III) associated with the precipitates (Figure 3c and Table S9). Additionally, the rate constants are likely of the same order of magnitude for As(III) and $MnOH^+$ oxidation by Fe(IV), e.g., $k_{MnOH^+} \geq 3.98 \times 10^5$, as suggested by the decrease in Mn(III) concentrations with increasing initial As(III) concentrations (Figure 3c) and decrease in As(V) concentrations with increasing initial Mn(II) concentrations (Figure 1A (A-3 and A-6) and Figure 1B (B-3 and B-6)).[15] Note that Mn(III)-substituted Fe oxides or any transient Mn(III) formation may also oxidize As(III),[36,38,59] but our data cannot be used to assess the importance of this mechanism.

Formation and Aggregation of Fe(III) Polymers Drive As(V) Removal. The large fraction of the polymer phase identified by Fe K-edge EXAFS spectroscopy across all samples (36−100%, Table S6) suggests that the As(V)−Fe(III) polymers in the dissolved phase are either the same or a precursor to the polymers identified in the solid phase. Transmission electron microscopy (TEM) analyses on samples collected before filtration (Figure S12) showed no difference in crystallinity over time. Instead, the amorphous precipitates showed similar morphologies after 13 and 32 min of EC and differed only by the length of the "Fe chains", thus suggesting that the polymers in the solid phase form from those in the dissolved phase.

Polymer aggregation depends on pH, initial As concentrations, and the presence of Mn, as shown by differences in the rate of As(V) removal from solution (Figure 1) and experiments using 0.02 μm filters (Figure S3). Overall, lower pH and the presence of Mn favored Fe(III) polymer aggregation, as can be seen from the smaller concentrations of dissolved Fe (Figure 2 and Table S8). This can be explained by charge-screening effects, wherein Mn(II) can enhance (i) Fe(III) polymerization and/or (ii) destabilization of the As(V)−Fe(III) polymers, as has been observed for Ca^{2+}.[16,17,52] Finally, aggregation may also be enhanced by the formation of more crystalline precipitates (e.g., Fh) once all of the As has been trapped in the polymer phase. The formation of As−Fe polymers in the dissolved phase can limit As removal, especially in groundwaters containing high As concentrations or other oxyanions compared to the added Fe concentrations. This problem can be addressed either by adding divalent cations such as Ca^{2+}, increasing the waiting time (especially at alkaline pH values), or using higher Fe production rates to attain As/Fe ratios $\ll 0.5$.

Sorption of As and Mn—Impact of Mn Incorporation on the Reactivity of the Fe(III) (Oxyhydr)oxides Formed by EC. The fraction of the As(V)−Fe(III) polymer present in all of the samples was sufficient to remove all As(V). However, our data do not provide unequivocal evidence that As was retained exclusively in the polymer phase because As(V) forms binuclear corner-sharing complexes on both the polymer phase and Fh. Additionally, the affinity of As(III) for the polymer phase versus Fh is unknown in the pH 8.5 10As100Mn and 100As100Mn samples. Lastly, while Mn(III) incorporation into the polymer phase cannot be excluded, its incorporation more likely occurs in Fh rather than the polymer as suggested by the presence of a second shell in the Mn K-edge EXAFS spectra. Given these limitations, we discuss the impact of Mn on As removal from solution with no assumption regarding the distribution of As between the Fe(III) polymers and Mn(III)-substituted Fh.

The incorporation of Mn(III) into Fe(III) oxyhydroxides at levels of up to 2% (mol Mn(III) mol^{-1} Fe(III)) had no apparent influence on As removal at pH 4.5 and 6.5. For these conditions, As removal was driven by the oxidation state of As in the dissolved phase—As(V) at pH 4.5 and As(III) at pH 6.5, where As(III) sorption by Fe(III) precipitates is less favorable than As(V) sorption at circumneutral pH values (Figure S13). At pH 8.5, the incorporation of 15 and 8% Mn(III) (mol Mn(III) mol^{-1} $Fe(III)_{solid}$) in the 10As100Mn and 100As100Mn experiments modified the sorption properties of the precipitates, likely through a change in the pH_{PZC}. Previous studies have shown that the pH_{PZC} values of Mn-substituted Fe oxides can decrease by 1−2 pH units relative to their pure counterparts (Table S10).[36−38] Such a decrease in the surface charge of the EC precipitates would favor As(V) sorption as well as charge-screening by Mn(II). This interpretation is consistent with the $As/Fe(III)_{solid}$ and $Mn(II):Fe(III)_{solid}$ ratios of 0.04 to 0.30 and 0.10 to 0.16, respectively, measured in the 10As0Mn and 100As100Mn experiments. The initial As(III):Mn(II) ratio in solution is thus an important parameter in EC systems at alkaline pH values, as it controls the composition and surface charge of the precipitates and thus As removal. Complementary experiments could be pursued to determine the $Mn(III)/Fe(III)_{solid}$ ratio at which As removal is favorable/unfavorable as well as the affinity of As(III) and As(V) for precipitates with varying amounts of Mn(III) incorporation.

Technical and Environmental Implications. This study provides a detailed analysis of the coupled redox transformations of As, Mn, and Fe. At acidic pH values, As(III) outcompetes Mn(II) for the reactive oxidants and the resulting As(V)−Fe(III) polymers aggregate readily. This aggregation appears to be driven by multiple factors, including low pH and the presence of Mn(II). At alkaline pH values, instead, As(III) and Mn(II) compete for the reactive oxidants, as evidenced by the persistence of As(III) in solution and the accumulation of Mn(III) in the solid phase. Nonetheless, extensive As removal of As(III), As(V), and Mn(II) was achieved due to the formation of As(V)−Fe(III) polymers and mixed Mn(III)−Fe(III) ferrihydrite-like precipitates. Similarly to pH 8.5, at pH 6.5, As(III) persisted in solution and As was removed as a mixture of As(III) and As(V). However, little Mn(III) was found in the solid phase formed at pH 6.5. This result suggests that the redox recycling of Mn(III) is likely an operative mechanism that allows for the sorption of As(V) to the solid phase at pH 6.5.

While As removal was most efficient at pH 4.5, acidic groundwaters where As and Mn co-occur are not frequently observed,[19,28] although EC may be applicable for the treatment of mine-drainage waters. Waters containing both As and Mn at pH close to 6.5[18,28] could be treated by EC to remove As but not Mn.[18,28] Finally, the removal of both As and Mn from the dissolved phase may be achieved in alkaline waters containing Mn concentrations above 50 μM.[18,19] However, the competition between As and Mn for the reactive oxidant species must be accounted for in setting the EC operating conditions (i.e., Fe addition rate, EC time, and concentration of H_2O_2). In places where the use of H_2O_2 is impractical due to cost or supply chain constraints, removing As(III,V) in the presence of Mn with O_2 as the initial oxidant may require longer treatment times and different Fe(II) production rates. Note that Mn

https://dx.doi.org/10.1021/acs.est.9b07099
Environ. Sci. Technol. 2020, 54, 7165−7174

concentrations lower than those used in this study are usually found in groundwaters, which should decrease the impact of Mn on As removal. Finally, additional research is needed to quantify the influence of other redox-sensitive species on As removal. Organic matter, which contains both reducing and oxidizing moieties,[60] can participate in complex reactions with reactive oxidant species and adsorbs to Fe(III) precipitates.[61−63] This makes it likely that organic matter will impact both redox and sorption reactions fundamental to the operation of EC systems for As removal.

■ ASSOCIATED CONTENT

Supporting Information

The Supporting Information is available free of charge at https://pubs.acs.org/doi/10.1021/acs.est.9b07099.

Additional details on the methods used in this study, including kinetics of As(III) and Mn(II) removal, chemical analyses, analysis of X-ray absorption spectra, and transmission electron microscopy; Fe(0) electrode composition; compilation of field measurements of As and Mn concentrations; schematic of the pathways for Fe, As, and Mn oxidation in an EC system; As removal as determined using 0.2 and 0.02 micron filters; percentage of Fe(IV) and OH• as a function of pH; As(III) speciation diagram; As, Fe, and Mn K-edge X-ray absorption spectra, including fit results; transmission electron micrographs; and surface complexation modeling of As(III, V) sorption by ferrihydrite (PDF)

■ AUTHOR INFORMATION

Corresponding Author

Jasquelin Peña − *Institute of Earth Surface Dynamics, University of Lausanne, Lausanne CH-1015, Switzerland;* orcid.org/0000-0001-7081-3873; Email: jasquelin.pena@unil.ch, pena@ucdavis.edu

Authors

Charlotte Catrouillet − *Institute of Earth Surface Dynamics, University of Lausanne, Lausanne CH-1015, Switzerland*

Sachiko Hirosue − *Institute of Earth Surface Dynamics, University of Lausanne, Lausanne CH-1015, Switzerland*

Nathalie Manetti − *Institute of Earth Surface Dynamics, University of Lausanne, Lausanne CH-1015, Switzerland*

Victor Boureau − *Interdisciplinary Center for Electron Microscopy, Ecole Polytechnique Fédérale de Lausanne, Lausanne CH-1015, Switzerland;* orcid.org/0000-0001-6251-5892

Complete contact information is available at: https://pubs.acs.org/10.1021/acs.est.9b07099

Notes

The authors declare no competing financial interest.

■ ACKNOWLEDGMENTS

This work was funded by the Swiss National Science Foundation (200021_169555). We are grateful to Laetitia Monbaron and Micaela Faria for laboratory support and ICP-OES analyses, and Jean-Claude Lavanchy for X-ray fluorescence analyses. We thank Dr. Case M. van Genuchten for valuable discussions as well as Jantina van der Meer and Dr. Sharon Bone for technical support and helpful discussion regarding the identification of the As(V)−Fe(III) polymers. We thank Ryan Davis, Cynthia Pathy, Risa Benwell, and Dr. Debra Hausladen for technical support at the Stanford Synchrotron Radiation Facility (SSRL). Use of the Stanford Synchrotron Radiation Lightsource, SLAC National Accelerator Laboratory, is supported by the U.S. Department of Energy, Office of Science, Office of Basic Energy Sciences.

■ REFERENCES

(1) Shan, Y.; Mehta, P.; Perera, D.; Varela, Y. *Cost and Efficiency of Arsenic Removal from Groundwater: A Review*; United Nations University Institute for Water, Environment and Health: Hamilton, Canada, 2018.

(2) Amrose, S. E.; Bandaru, S. R. S.; Delaire, C.; van Genuchten, C. M.; Dutta, A.; DebSarkar, A.; Orr, C.; Roy, J.; Das, A.; Gadgil, A. J. Electro-chemical arsenic remediation: Field trials in West Bengal. *Sci. Total Environ.* **2014**, *488−489*, 539−546.

(3) Lakshmipathiraj, P.; Prabhakar, S.; Raju, G. B. Studies on the electrochemical decontamination of wastewater containing arsenic. *Sep. Purif. Technol.* **2010**, *73*, 114−121.

(4) Nidheesh, P. V.; Singh, T. S. A. Arsenic removal by electrocoagulation process: Recent trends and removal mechanism. *Chemosphere* **2017**, *181*, 418−432.

(5) Song, P.; Yang, Z.; Zeng, G.; Yang, X.; Xu, H.; Wang, L.; Xu, R.; Xiong, W.; Ahmad, K. Electrocoagulation treatment of arsenic in wastewaters: A comprehensive review. *Chem. Eng. J.* **2017**, *317*, 707−725.

(6) Ratna Kumar, P.; Chaudhari, S.; Khilar, K. C.; Mahajan, S. P. Removal of arsenic from water by electrocoagulation. *Chemosphere* **2004**, *55*, 1245−1252.

(7) Tong, M.; Yuan, S.; Wang, Z.; Luo, M.; Wang, Y. Electrochemically induced oxidative removal of As(III) from groundwater in a dual-anode sand column. *J. Hazard. Mater.* **2016**, *305*, 41−50.

(8) Wan, W.; Pepping, T. J.; Banerji, T.; Chaudhari, S.; Giammar, D. E. Effects of water chemistry on arsenic removal from drinking water by electrocoagulation. *Water Res.* **2011**, *45*, 384−392.

(9) Wang, J. W.; Bejan, D.; Bunce, N. J. Removal of Arsenic from Synthetic Acid Mine Drainage by Electrochemical pH Adjustment and Coprecipitation with Iron Hydroxide. *Environ. Sci. Technol.* **2003**, *37*, 4500−4506.

(10) Li, L.; van Genuchten, C. M.; Addy, S. E. A.; Yao, J.; Gao, N.; Gadgil, A. J. Modeling As(III) Oxidation and Removal with Iron Electrocoagulation in Groundwater. *Environ. Sci. Technol.* **2012**, *46*, 12038−12045.

(11) Pan, C.; Troyer, L. D.; Catalano, J. G.; Giammar, D. E. Dynamics of Chromium(VI) Removal from Drinking Water by Iron Electrocoagulation. *Environ. Sci. Technol.*. **2016**, *50*, 13502−13510.

(12) Pan, C.; Troyer, L. D.; Liao, P.; Catalano, J. G.; Li, W.; Giammar, D. E. Effect of Humic Acid on the Removal of Chromium(VI) and the Production of Solids in Iron Electrocoagulation. *Environ. Sci. Technol.* **2017**, *51*, 6308−6318.

(13) van Genuchten, C. M.; Addy, S. E. A.; Peña, J.; Gadgil, A. J. Removing Arsenic from Synthetic Groundwater with Iron Electrocoagulation: An Fe and As K-Edge EXAFS Study. *Environ. Sci. Technol.* **2012**, *46*, 986−994.

(14) van Genuchten, C. M.; Bandaru, S. R. S.; Surorova, E.; Amrose, S. E.; Gadgil, A. J.; Peña, J. Formation of macroscopic surface layers on Fe(0) electrocoagulation electrodes during an extended field trial of arsenic treatment. *Chemosphere* **2016**, *153*, 270−279.

(15) Hug, S. J.; Leupin, O. Iron-catalyzed oxidation of arsenic(III) by oxygen and by hydrogen peroxide: pH-dependent formation of oxidants in the Fenton reaction. *Environ. Sci. Technol.* **2003**, *37*, 2734−2742.

(16) van Genuchten, C. M.; Gadgil, A. J.; Peña, J. Fe(III) Nucleation in the Presence of Bivalent Cations and Oxyanions Leads to Subnanoscale 7 Å Polymers. *Environ. Sci. Technol.* **2014**, *48*, 11828−11836.

(17) van Genuchten, C. M.; Peña, J.; Amrose, S. E.; Gadgil, A. J. Structure of Fe(III) precipitates generated by the electrolytic

dissolution of Fe(0) in the presence of groundwater ions. *Geochim. Cosmochim. Acta* **2014**, *127*, 285−304.
(18) Buschmann, J.; Berg, M.; Stengel, C.; Sampson, M. L. Arsenic and Manganese Contamination of Drinking Water Resources in Cambodia: Coincidence of Risk Areas with Low Relief Topography. *Environ. Sci. Technol.* **2007**, *41*, 2146−2152.
(19) de Meyer, C. M. C.; Rodríguez, J. M.; Carpio, E. A.; García, P. A.; Stengel, C.; Berg, M. Arsenic, manganese and aluminum contamination in groundwater resources of Western Amazonia (Peru). *Sci. Total Environ.* **2017**, *607−608*, 1437−1450.
(20) Gillispie, E. C.; Andujar, E.; Polizzotto, M. L. Chemical controls on abiotic and biotic release of geogenic arsenic from Pleistocene aquifer sediments to groundwater. *Environ. Sci.: Processes Impacts* **2016**, *18*, 1090−1103.
(21) Halim, M. A.; Majumder, R. K.; Rasul, G.; Hirosiro, Y.; Sasaki, K.; Shimada, J.; Jinno, K. Geochemical Evaluation of Arsenic and Manganese in Shallow Groundwater and Core Sediment in Singair Upazila, Central Bangladesh. *Arabian J. Sci. Eng.* **2014**, *39*, 5585−5601.
(22) Hossain, M. B.; Jahiruddin, M.; Panaullah, G. M.; Loeppert, R. H.; Islam, M. R.; Duxbury, J. M. Spatial variability of arsenic concentration in soils and plants, and its relationship with iron, manganese and phosphorus. *Environ. Pollut.* **2008**, *156*, 739−744.
(23) Hug, S. J.; Gaertner, D.; Roberts, L. C.; Schirmer, M.; Ruettimann, T.; Rosenberg, T. M.; Badruzzaman, A. B. M.; Ashraf Ali, M. Avoiding high concentrations of arsenic, manganese and salinity in deep tubewells in Munshiganj District, Bangladesh. *Appl. Geochem.* **2011**, *26*, 1077−1085.
(24) Nguyen, V. A.; Bang, S.; Viet, P. H.; Kim, K.-W. Contamination of groundwater and risk assessment for arsenic exposure in Ha Nam province, Vietnam. *Environ. Int.* **2009**, *35*, 466−472.
(25) Rahman, M. M.; Dong, Z.; Naidu, R. Concentrations of arsenic and other elements in groundwater of Bangladesh and West Bengal, India: Potential cancer risk. *Chemosphere* **2015**, *139*, 54−64.
(26) Rowland, H. A. L.; Omoregie, E. O.; Millot, R.; Jimenez, C.; Mertens, J.; Baciu, C.; Hug, S. J.; Berg, M. Geochemistry and arsenic behaviour in groundwater resources of the Pannonian Basin (Hungary and Romania). *Appl. Geochem.* **2011**, *26*, 1−17.
(27) Sankar, M. S.; Vega, M. A.; Defoe, P. P.; Kibria, M. G.; Ford, S.; Telfeyan, K.; Neal, A.; Mohajerin, T. J.; Hettiarachchi, G. M.; Barua, S.; Hobson, C.; Johannesson, K.; Datta, S. Elevated arsenic and manganese in groundwaters of Murshidabad, West Bengal, India. *Sci. Total Environ.* **2014**, *488-489*, 570−579.
(28) Sthiannopkao, S.; Kim, K. W.; Sotham, S.; Choup, S. Arsenic and manganese in tube well waters of Prey Veng and Kandal Provinces, Cambodia. *Appl. Geochem.* **2008**, *23*, 1086−1093.
(29) van Genuchten, C. M.; Peña, J. Mn(II) Oxidation in Fenton and Fenton Type Systems: Identification of Reaction Efficiency and Reaction Products. *Environ. Sci. Technol.* **2017**, *51*, 2982−2991.
(30) Hansel, C. M.; Zeiner, C. A.; Santelli, C. M.; Webb, S. M. Mn(II) oxidation by an ascomycete fungus is linked to superoxide production during asexual reproduction. *Proc. Natl. Acad. Sci. U.S.A.* **2012**, *109*, 12621−12625.
(31) Learman, D.; Voelker, B.; Madden, A.; Hansel, C. Constraints on superoxide mediated formation of manganese oxides. *Front. Microbiol.* **2013**, *4*, 262.
(32) Learman, D. R.; Voelker, B. M.; Vazquez-Rodriguez, A. I.; Hansel, C. M. Formation of manganese oxides by bacterially generated superoxide. *Nat. Geosci.* **2011**, *4*, 95.
(33) Learman, D. R.; Wankel, S. D.; Webb, S. M.; Martinez, N.; Madden, A. S.; Hansel, C. M. Coupled biotic−abiotic Mn(II) oxidation pathway mediates the formation and structural evolution of biogenic Mn oxides. *Geochim. Cosmochim. Acta* **2011**, *75*, 6048−6063.
(34) Nico, P. S.; Anastasio, C.; Zasoski, R. J. Rapid photo-oxidation of Mn(II) mediated by humic substances. *Geochim. Cosmochim. Acta* **2002**, *66*, 4047−4056.
(35) Reisz, E.; Leitzke, A.; Jarocki, A.; Irmscher, R.; von Sonntag, C. Permanganate formation in the reactions of ozone with Mn(II): a mechanistic study. *J. Water Supply: Res. Technol.–AQUA* **2008**, *57*, 451−464.
(36) Li, J.; Gyoten, H.; Sonoda, A.; Feng, Q.; Xue, M. Removal of trace arsenic to below drinking water standards using a Mn-Fe binary oxide. *RSC Adv.* **2017**, *7*, 1490−1497.
(37) Nikić, J.; Agbaba, J.; Watson, M.; Maletić, S.; Molnar Jazić, J.; Dalmacija, B. Adsorption mechanism of As(V) and As(III) on Fe−Mn binary oxides in synthetic and real water matrices. *Water Sci. Technol.: Water Supply* **2016**, 992−1001.
(38) Sun, X. H.; Doner, H. E.; Zavarin, M. Spectroscopy study of arsenite [As(III)] oxidation on Mn-substituted goethite. *Clay Clay Miner.* **1999**, *47*, 474−480.
(39) Manning, B. A.; Fendorf, S. E.; Bostick, B.; Suarez, D. L. Arsenic(III) oxidation and arsenic(V) adsorption reactions on synthetic birnessite. *Environ. Sci. Technol.* **2002**, *36*, 976−981.
(40) Parikh, S. J.; Lafeerty, B. J.; Meade, T. G.; Sparks, D. L. Evaluating Environmental Influences on As-III Oxidation Kinetics by a Poorly Crystalline Mn-Oxide. *Environ. Sci. Technol.* **2010**, *44*, 3772−3778.
(41) Scott, M. J.; Morgan, J. J. Reactions at Oxide Surfaces 1. Oxidation of As(III) by Synthetic Birnessite. *Environ. Sci. Technol.* **1995**, *29*, 1898−1905.
(42) Dixit, S.; Hering, J. G. Comparison of arsenic(V) and arsenic(III) sorption onto iron oxide minerals: Implications for arsenic mobility. *Environ. Sci. Technol.* **2003**, *37*, 4182−4189.
(43) Hineman, A.*Determination of As, Se and Hg in Waters by Hydride Generation/Cold Vapor Atomic Absorption Spectroscopy*; Perkin Elmer: Ontario, Canada, 2011.
(44) Millero, F. J.; Sotolongo, S.; Izaguirre, M. The oxidation kinetics of Fe(II) in seawater. *Geochim. Cosmochim. Acta* **1987**, *51*, 793−801.
(45) Balmer, M. E.; Sulzberger, B. Atrazine degradation in irradiated iron oxalate systems: Effects of pH and oxalate. *Environ. Sci. Technol.* **1999**, *33*, 2418−2424.
(46) Wiegand, H. L.; Orths, C. T.; Kerpen, K.; Lutze, H. V.; Schmidt, T. C. Investigation of the Iron-Peroxo Complex in the Fenton Reaction: Kinetic Indication, Decay Kinetics, and Hydroxyl Radical Yields. *Environ. Sci. Technol.* **2017**, *51*, 14321−14329.
(47) Litter, M. I.; Slodowicz, M. An overview on heterogeneous Fenton and photoFenton reactions using zerovalent iron materials. *J. Adv. Oxid. Technol.* **2017**, *20*, No. 164.
(48) Webb, S. M.; Dick, G. J.; Bargar, J. R.; Tebo, B. M. Evidence for the presence of Mn(III) intermediates in the bacterial oxidation of Mn(II). *Proc. Natl. Acad. Sci. U.S.A.* **2005**, *102*, 5558−5563.
(49) Hu, Y. D.; Lee, B.; Bell, C.; Jun, Y. S. Environmentally Abundant Anions Influence the Nucleation, Growth, Ostwald Ripening, and Aggregation of Hydrous Fe(III) Oxides. *Langmuir* **2012**, *28*, 7737−7746.
(50) Shi, Q. T.; Jing, C. Y.; Meng, X. G. Competing Interactions of As Adsorption and Fe(III) Polymerization during Ferric Coprecipitation Treatment. *Environ. Sci. Technol.* **2018**, *52*, 7343−7350.
(51) Pham, A. N.; Rose, A. L.; Feitz, A. J.; Waite, T. D. Kinetics of Fe(III) precipitation in aqueous solutions at pH 6.0-9.5 and 25 degrees C. *Geochim. Cosmochim. Acta* **2006**, *70*, 640−650.
(52) Senn, A.-C.; Kaegi, R.; Hug, S. J.; Hering, J. G.; Mangold, S.; Voegelin, A. Composition and structure of Fe(III)-precipitates formed by Fe(II) oxidation in water at near-neutral pH: Interdependent effects of phosphate, silicate and Ca. *Geochim. Cosmochim. Acta* **2015**, *162*, 220−246.
(53) Owings, S. M.; Luther, G. W.; Taillefert, M. Development of a rate law for arsenite oxidation by manganese oxides. *Geochim. Cosmochim. Acta* **2019**, *250*, 251−267.
(54) Baral, S.; Lume-Pereira, C.; Janata, E.; Henglein, A. Chemistry of colloidal manganese oxides. 3. Formation in the reaction of hydroxyl radicals with manganese(2+) ions. *J. Phys. Chem. A.* **1986**, *90*, 6025−6028.
(55) Dorfman, L. M. A.; Gerald, E. *Reactivity of the Hydroxyl Radical in Aqueous Solutions*; National Standard Reference Data System, 1973; p 71.

https://dx.doi.org/10.1021/acs.est.9b07099
Environ. Sci. Technol. 2020, 54, 7165−7174

(56) Isaure, M.-P.; Laboudigue, A.; Manceau, A.; Sarret, G.; Tiffreau, C.; Trocellier, P.; Lamble, G.; Hazemann, J.-L.; Chateigner, D. Quantitative Zn speciation in a contaminated dredged sediment by μ-PIXE, μ-SXRF, EXAFS spectroscopy and principal component analysis. *Geochim. Cosmochim. Acta* **2002**, *66*, 1549−1567.
(57) Hiemstra, T.; Mendez, J. C.; Li, J. Evolution of the reactive surface area of ferrihydrite: time, pH, and temperature dependency of growth by Ostwald ripening. *Environ. Sci.: Nano* **2019**, *6*, 820−833.
(58) Siebecker, M.; Madison, A. S.; Luther, G. W. Reduction Kinetics of Polymeric (Soluble) Manganese (IV) Oxide (MnO2) by Ferrous Iron (Fe2+). *Aquat. Geochem.* **2015**, *21*, 143−158.
(59) Zhang, G.; Liu, H.; Qu, J.; Jefferson, W. Arsenate uptake and arsenite simultaneous sorption and oxidation by Fe−Mn binary oxides: Influence of Mn/Fe ratio, pH, Ca2+, and humic acid. *J. Colloid Interface Sci.* **2012**, *366*, 141−146.
(60) Walpen, N.; Getzinger, G. J.; Schroth, M. H.; Sander, M. Electron-Donating Phenolic and Electron-Accepting Quinone Moieties in Peat Dissolved Organic Matter: Quantities and Redox Transformations in the Context of Peat Biogeochemistry. *Environ. Sci. Technol.* **2018**, *52*, 5236−5245.
(61) Mikutta, C.; Frommer, J.; Voegelin, A.; Kaegi, R.; Kretzschmar, R. Effect of citrate on the local Fe coordination in ferrihydrite, arsenate binding, and ternary arsenate complex formation. *Geochim. Cosmochim. Acta* **2010**, *74*, 5574−5592.
(62) Mikutta, C.; Kretzschmar, R. Spectroscopic Evidence for Ternary Complex Formation between Arsenate and Ferric Iron Complexes of Humic Substances. *Environ. Sci. Technol.* **2011**, *45*, 9550−9557.
(63) Sharma, P.; Ofner, J.; Kappler, A. Formation of Binary and Ternary Colloids and Dissolved Complexes of Organic Matter, Fe and As. *Environ. Sci. Technol.* **2010**, *44*, 4479−4485.

https://dx.doi.org/10.1021/acs.est.9b07099
Environ. Sci. Technol. 2020, 54, 7165−7174